The Journal of Chemical Physics

Electronic density of states of fluid mixtures in the single superchain/effective medium approximation

Cite as: J. Chem. Phys. **104**, 5244 (1996); https://doi.org/10.1063/1.471151
Submitted: 09 November 1995 . Accepted: 20 December 1995 . Published Online: 31 August 1998

E. Lomba, and J. L. López-Martín

Electronic density of states of fluid mixtures in the single superchain/effective medium approximation

E. Lomba and J. L. López-Martín
Instituto de Química Física Rocasolano, CSIC, Serrano 119, E-28006 Madrid, Spain

(Received 9 November 1995; accepted 20 December 1995)

We introduce a straightforward extension to binary mixtures of Logan and Winn's formalism for the determination of the electronic density of states in disordered systems. Solutions obtained in the single superchain/effective medium approximation are also presented, and though reflecting the limitations intrinsic to the linear nature of this approximation, computer simulation results for the mixture of asymmetric hard spheres are reproduced quite satisfactorily. In particular the dependence of the band shape (and the width of the band gap) on the particle size asymmetry is correctly accounted for. The implementation of efficient integral equation algorithms to deal with complex Ornstein–Zernike equations also constitutes one of the key contributions of this work and is therefore treated in depth. © *1996 American Institute of Physics.* [S0021-9606(96)50812-5]

I. INTRODUCTION

In a recent work, the authors in collaboration with Høye[1] introduced a theory for the determination of the band structure (or frequency spectrum) of binary fluid mixtures and two-band fluids with quenched translational degrees of freedom in the tight-binding Hamiltonian level of description. This theory was solved for fully symmetric mixtures in the mean spherical approximation (MSA) and in a nonlinear approximation developed earlier by Høye and Lomba.[2] The extension of both approaches to asymmetric mixtures (i.e., those composed of particles of unequal diameters) or mixtures where the standard mixing rule for crossed interactions is not fulfilled, though feasible, is by no means straightforward.

On the other hand, Logan and Winn's formalism[3] when solved beyond the simple MSA for two-band fluids and related systems presents a nontrivial numerical problem, since it requires the solution of a complex Ornstein–Zernike-like (OZ) equation coupled with a nonlinear algebraic equation (for each energy value to be considered). Daunting as it might look, once this problem is solved, Logan and Winn's formalism has the advantage that the solution procedure can deal with any type of transfer matrix element of the tight-binding Hamiltonians and any sort of molecular interaction determining the spatial distribution of the quenched system.

Therefore, we decided first to formulate the expressions that yield the electronic density of states (DOS) in mixtures within Logan and Winn's formalism and then make use of the most efficient integral equation-solver algorithms to develop an approach capable of tackling this highly nontrivial numerical problem. The theory was solved in its simplest linear approximation beyond the MSA, namely the single superchain/effective medium approximation (SSCA/EMA), which incorporates the effect of spatial correlations,[4] yielding correct first and second moments of the DOS. Several Monte Carlo simulations with direct diagonalization and averaging of the tight binding Hamiltonian were also performed to assess the quality of the theory. The extension to multicomponent fluids is immediate, whereas the treatment of mixtures of multiband fluids which is formally straightforward, is considerably more involved from the standpoint of its numerical solution. Work in this direction is in progress.

The rest of the paper can be sketched as follows. In Sec. II we introduce the expressions that determine the DOS in a mixture of one-band fluids, i.e., a fluid composed of two types of particles with only one excitation level. In Sec. III we summarize the numerical procedures required to solve the proposed equations, and analyze and discuss the results obtained for a test model of asymmetric hard-sphere mixtures with Yukawa-type transfer matrix elements defining the tight-binding Hamiltonian.

II. DENSITY OF ELECTRONIC STATES IN BINARY MIXTURES

In a system composed of N_α particles of type α (labeled $1,2,\ldots,N_\alpha$) and $N_\beta = N - N_\alpha$ particles of type β $(N_\alpha+1,\ldots,N)$, with each particle type having a single excitation level ε_α or ε_β, the tight-binding Hamiltonian is given by

$$H = \sum_{i=1}^{N_\alpha} \varepsilon_{i\alpha} c_{i\alpha}^{+} c_{i\alpha} + \sum_{N_\alpha+1}^{N} \varepsilon_{i\beta} c_{i\beta}^{+} c_{i\beta} + \sum_{i,j\leqslant N_\alpha} V_{ij}^{\alpha\alpha} c_{i\alpha}^{+} c_{j\alpha} + \sum_{i,j>N_\beta} V_{ij}^{\beta\beta} c_{i\beta}^{+} c_{j\beta} + \sum_{i\leqslant N_\alpha \leqslant j} V_{ij}^{\alpha\beta} c_{i\alpha}^{+} c_{j\beta} + \sum_{j\leqslant N_\alpha \leqslant i} V_{ij}^{\beta\alpha} c_{i\beta}^{+} c_{j\alpha}, \tag{2.1}$$

where $c_{i\alpha}^{+}(c_{i\alpha})$ is a creation (annihilation) operator for the one-electron state associated with the level α on the particle i (which is type α) located at R_i, $\varepsilon_{i\alpha}$ is the zero-order energy of level α in the particle of α type (and correspondingly for β-type particles), and $V_{ij}^{\alpha\alpha}$, $V_{ij}^{\alpha\beta}$, $V_{ij}^{\beta\alpha}$, $V_{ij}^{\beta\beta}$ are the transfer matrix elements between sites i,j which differ according to the particle types involved in the electronic transfer.

It is easy to see that this two-component mixture of one-band fluids, with energy levels ε_α and ε_β and transfer matrix

 0021-9606/96/104(13)/5244/7/$10.00

elements $V^{\alpha\beta}$, can be understood as a particular case of the two-band one-component fluid, in which there are two energy levels ε_α and ε_β associated with each site. This latter system has been studied exhaustively in Refs. 5 and 6 and we refer the reader to these works for a more detailed presentation of the concepts and terminology employed hereafter. As explained in Refs. 5 and 6, the relevant quantities for the determination of the energy DOS are the average diagonal Green's functions of the tight-binding Hamiltonian (2.1), $\bar{G}^{\alpha\alpha}$, and $\bar{G}^{\beta\beta}$. Also, in a crucial quantity like the off-diagonal Green's function $\bar{G}^{\alpha\beta}(ij)$, one must take into account the fact that an α (or β) energy level can only occur that is associated with a particle of α (or β) type. Therefore the end stages in the composite interaction graphs contributing to the average diagonal Green's function (see Sec. II in Ref. 5) must correspond to $V^{\alpha\lambda}(ik)$ and $V^{\lambda'\beta}(k'j)$ with particles i and j of type α and β, respectively. Also, the average diagonal Green's functions $\bar{G}^{\alpha\beta}(z)$, diagramatically corresponds to a loop (the two end stages are associated with the same particle) and thereby must be restricted to $\bar{G}^{\alpha\alpha}(z)$ and $\bar{G}^{\beta\beta}(z)$. Each ρ factor occurring at each field point in the expansion of the Green's function and related quantities must now be replaced to take into account the introduction of an additional degree of freedom representing the particle type, that is, one must perform the substitution

$$\int \rho(i)d\mathbf{i} \rightarrow \sum_\lambda \int \rho_\lambda(i)d\mathbf{i}, \tag{2.2}$$

where the λ index runs over the components of the mixture. More explicitly we can define the diagonal Green's function as[7]

$$\rho_\alpha \bar{G}^{\alpha\alpha}(1) = \left\langle \sum_{i_\alpha} G_{i_\alpha i_\alpha}\delta(i-1) \right\rangle \tag{2.3}$$

and the off-diagonal Green's function as

$$\rho_\alpha \rho_\beta \bar{G}^{\alpha\beta}(12) = \left\langle \sum_{i_\alpha j_\beta} G_{i_\alpha j_\beta}\delta(i-1)\,\delta(j-2) \right\rangle. \tag{2.4}$$

The sums run over all particles i_α of species α. Averaging the Green's function equation [see Eq. (7) in Ref. 5], one gets

$$V\rho_\alpha z_\alpha \bar{G}^{\alpha\alpha} = N_\alpha + V\rho_\alpha \sum_\lambda \rho_\lambda \int V^{\alpha\lambda}(12)\bar{G}^{\lambda\alpha}(21)d2 \tag{2.5}$$

from which

$$z_\alpha \bar{G}^{\alpha\alpha} = 1 + \sum_\lambda \int V^{\alpha\lambda}(12)\rho_\lambda(2)\bar{G}^{\lambda\alpha}(21)d2, \tag{2.6}$$

where z_α (z_β) represents the energy associated with the α (β) levels. Now the equation that connects the off-diagonal Green's function with the diagonal Green's function [Eq. (8) in Ref. 5] must be modified to take into account that only $\bar{G}^{\alpha\alpha}(z)$ and $\bar{G}^{\beta\beta}(z)$ occur, leading to

$$\bar{G}^{\alpha\beta}(12) = \bar{G}^{\alpha\alpha}H^{\alpha\beta}(12)\bar{G}^{\beta\beta}, \tag{2.7}$$

where $H^{\alpha\beta}$ is some sort of correlation function that fulfills an OZ-like equation.[5] Equation (2.7) when inserted into Eq. (2.6) gives

$$z_\alpha \bar{G}^{\alpha\alpha} = 1 + \bar{G}^{\alpha\alpha}\sum_\lambda \rho_\lambda \bar{G}^{\lambda\lambda} \int V^{\alpha\lambda}(12)H^{\lambda\alpha}(21)d2 \tag{2.8}$$

and likewise for $z_\beta \bar{G}^{\beta\beta}$. Similarly the OZ-like equation satisfied by $H^{\alpha\beta}$ will now read

$$H^{\alpha\beta}(12) = C^{\alpha\beta}(12) + \sum_\lambda \rho_\lambda \bar{G}^{\lambda\lambda} \int H^{\alpha\lambda}(13)C^{\lambda\alpha}(32)d3, \tag{2.9}$$

where once more $C^{\alpha\beta}$ is topologically related to the direct correlation function in fluid theory. As to the closure relation, since the nature of the particle imposes the type of energy level appearing in each site, the SSCA/EMA will read

$$C^{\alpha\beta}(12) = g_{\alpha\beta}(r)V^{\alpha\beta}(12) + h_{\alpha\beta}(r) \times [H^{\alpha\beta}(12) - C^{\alpha\beta}(12)], \tag{2.10}$$

where $g_{\alpha\beta}(r)$ is the pair distribution function between particles of α and β type, and $h_{\alpha\beta} = g_{\alpha\beta} - 1$. The nonlinear closure proposed by Logan and Winn[3] can also be readily extended to the mixture case. By including the multihopping contribution from the first series of diagrams that appear in the expansion of $C^{\alpha\beta}$ (see Fig. 1 in Ref. 5), one gets

$$C^{\alpha\beta}(12) = g_{\alpha\beta}(r)[V^{\alpha\beta}(12) + V^{\alpha\beta}(12)\bar{G}^{\beta\beta}V^{\beta\alpha}(21)\bar{G}^{\alpha\alpha}V^{\alpha\beta}(12) + \cdots] + h_{\alpha\beta}(12)[H^{\alpha\beta} - C^{\alpha\beta}], \tag{2.11}$$

which can be resumed to yield

$$C^{\alpha\beta}(12) = g_{\alpha\beta}(r)\frac{V^{\alpha\beta}(12)}{1 - \bar{G}^{\alpha\alpha}(z)V^{\alpha\beta}(12)\bar{G}^{\beta\beta}(z)V^{\beta\alpha}(12)} + h_{\alpha\beta}(12)[H^{\alpha\beta} - C^{\alpha\beta}]. \tag{2.12}$$

This nonlinear closure, though extremely attractive,[8] introduces an enormous multiplicity of solutions in complex space, and this complicates the numerics to a great extent. Therefore we do not pursue this approach further in this work. Finally, the average DOS must be evaluated from the weighted contribution of each species, i.e.,

$$D(E) = \frac{-1}{\pi}\lim_{\epsilon \rightarrow 0^+} \{\rho_\alpha \,\mathrm{Im}[\bar{G}^{\alpha\alpha}(E + i\epsilon)] + \rho_\beta \,\mathrm{Im}[\bar{G}^{\beta\beta}(E + i\epsilon)]\}/(\rho_\alpha + \rho_\beta). \tag{2.13}$$

The DOS is then fully determined by the set of nonlinear algebraic Eqs. (2.8) coupled with the set of integral equations formed by Eqs. (2.9) and (2.10). This system has to be solved for each energy and by simple insertion of the Green's function into Eq. (2.13) the DOS is obtained.

III. THE NUMERICAL PROCEDURE. DISCUSSION OF RESULTS

The calculations presented in this paper involve both the simulation and solution of complex integral equations. As for the Monte Carlo simulation we have followed the scheme indicated in Ref. 1 for equal-size hard sphere mixtures. In this case we have run Monte Carlo simulations for a variety of size ratios $\sigma_\beta/\sigma_\alpha$ (1:1, 1:1.25, and 1:1.92). In Ref. 1 it was seen that for the relatively low densities considered therein it was sufficient to average one **k** vector of the dispersion relation [$\mathbf{k}=(0,0,0)$, i.e., the Γ point] to obtain an adequate representation of the DOS. Here however, the packing fractions are relatively high [in particular for the largest asymmetry, for which $\eta=\pi(\rho_\alpha\sigma_\alpha^3+\rho_\beta\sigma_\beta^3)/6=0.42\sigma_\alpha^3$], and following other authors[9–11] we have performed the diagonalization of the tight-binding Hamiltonian as defined in Eq. (4.3) of Ref. 1 but including the following **k** vectors:

$$\Gamma:(\pi/L)(0,0,0), \qquad M:(\pi/L)(1,1,0),$$
$$X:(\pi/L)(1,0,0), \qquad R:(\pi/L)(1,1,1), \tag{3.1}$$

where L is the side of the simulation box.

The transfer matrix elements are now replaced by their Fourier transforms[9]

$$V^{jk}(\mathbf{k})=\sum_a \exp(\mathbf{ika})\mathbf{V}(|\mathbf{r_j}-\mathbf{r_k}+\mathbf{a}|), \tag{3.2}$$

where the summation ranges over three periodic cells adjacent to the central simulation cell along each perpendicular direction, i.e., the summation includes 26 replicas of the simulation cell. This implies that the minimum image convention is dropped. In Eq.(3.2), **a** is the unit cell vector and as in Ref. 1 the Yukawa transfer matrix elements are

$$V^{\alpha\beta}(R)=-(V_0^{\alpha\beta}/R)\exp(-a^{\alpha\beta}R), \tag{3.3}$$

where R is the interparticle separation and $a^{\alpha\beta}$ is a screening factor, which in all calculations presented in this work was set to $0.5\sigma_\alpha$. $V_0^{\alpha\beta}=V_0$ is also defined as energy units for simplicity, and $(\varepsilon_\alpha-\varepsilon_\beta)/V_0=1.0$, this means that the lowest excitation energy corresponds to β-type particles. With the use of a 500 particle sample, and generating 20 000 configurations with diagonalization of the Hamiltonian every 50 configurations, one gets reliable estimates. Figure 1 illustrates the effect of including a larger number of **k**-vectors in the averaging with respect to the single **k**-vector averages. Nonetheless the results for the higher anisotropy still show the effects of the finite number of the **k**-vectors included. It is obvious that the structure appearing at low energy is nothing but an artifact of this limitation.

As mentioned before the theoretical determination of the DOS involves the simultaneous numerical solution of a set of nonlinear algebraic equations coupled with an integral equation. As is customary in fluid integral equation theory, Eqs. (2.9) and (2.10) must be rewritten in terms of the difference $\gamma^{\alpha\beta}(12)=H^{\alpha\beta}(12)-C^{\alpha\beta}(12)$, and for convenience the Fourier transforms needed to evaluate the convolution in Eq. (2.9) should be scaled with the effective densities, by means of

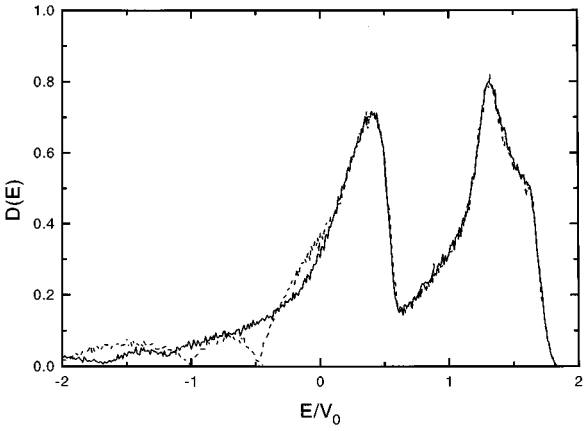

FIG. 1. Simulation results for the density of electronic states of a mixture of asymmetric hard spheres (size ratio 1:1.25) with a tight-binding Hamiltonian with Yukawa transfer matrix elements. The solid line corresponds to minimum-image results with averages over one **k** vector (the Γ point) and the dashed line shows the results of a four **k**-vector averaging over 27 replicas of the simulation cell.

$$k\tilde{f}^{\alpha\beta}(k)=4\pi(\rho_\alpha\bar{G}^{\alpha\alpha}\rho_\beta\bar{G}^{\beta\beta})^{1/2}\int rf(r)\sin kr\, dr \tag{3.4}$$

and

$$rf^{\alpha\beta}(r)=1/(2\pi^2)\frac{1}{(\rho_\alpha\bar{G}^{\alpha\alpha}\rho_\beta\bar{G}^{\beta\beta})^{1/2}}\int k\tilde{f}(k)\sin kr\, dk. \tag{3.5}$$

Thus Eq. (2.9) transforms into

$$\tilde{\mathbf{\Gamma}}(k)=\tilde{\mathbf{C}}^2(k)[\mathbf{I}+\tilde{\mathbf{C}}(k)]^{-1}, \tag{3.6}$$

where the elements of the matrices designate the different species, i.e., $[\tilde{\mathbf{C}}]^{\alpha\beta}=\tilde{C}^{\alpha\beta}$, $\tilde{C}^{\alpha\beta}(k)=k\tilde{c}^{\alpha\beta}(k)$, and $\tilde{\Gamma}^{\alpha\beta}(k)=k\tilde{\gamma}^{\alpha\beta}(k)$.

Also the SSCA/EMA closure now reads

$$C^{\alpha\beta}(12)=g_{\alpha\beta}(r)V^{\alpha\beta}(12)+h_{\alpha\beta}(r)\gamma^{\alpha\beta}(12). \tag{3.7}$$

Equations (3.6) and (3.7) can now be solved in complex space provided that $\bar{G}^{\alpha\alpha}$ and $\bar{G}^{\beta\beta}$ are known. We have found that the most efficient algorithm (as far as stability and convergence properties are concerned) is the one proposed by Ng[12] for the solution of OZ equations in charged systems. The stability is further increased by adding a mixing iterates step, to damp possible unstable oscillations. The algorithm can be summarized as follows: for a given set of consecutive estimates (obtained in the first place by simple substitution) γ_i, γ_{i+1}, γ_{i+2} (where the subscript denotes the iteration number), one stores its corresponding errors defined by

$$\delta\gamma_0^i=\sum_{j,\alpha,\beta}[\gamma_{i+2}^{\alpha\beta}(r_j)-\gamma_{i+1}^{\alpha\beta}(r_j)]^2,$$

$$\delta\gamma_1^i=\sum_{j,\alpha,\beta}[\gamma_{i+2}^{\alpha\beta}(r_j)-\gamma_{i+1}^{\alpha\beta}(r_j)][\gamma_{i+1}^{\alpha\beta}(r_j)-\gamma_i^{\alpha\beta}(r_j)],$$

$$\delta\gamma\,{}_2^i=\sum_{j,\alpha,\beta}\left[\gamma_{i+2}^{\alpha\beta}(r_j)-\gamma_{i+1}^{\alpha\beta}(r_j)\right]\left[\gamma_i^{\alpha\beta}(r_j)-\gamma_{i-1}^{\alpha\beta}(r_j)\right]. \tag{3.8}$$

An extrapolation is then used to determine the next γ_{i+3} for which one would expect $\delta\gamma\,{}_0^{i+1}=0$. This will force a quasi-quadratic convergence. It can be shown that the next estimate is defined by

$$\gamma_{i+3}^{\alpha\beta}=\gamma_{i+2}^{\alpha\beta}+c_1(\gamma_{i+1}^{\alpha\beta}-\gamma_{i+2}^{\alpha\beta})+c_2(\gamma_i^{\alpha\beta}-\gamma_{i+2}^{\alpha\beta}), \tag{3.9}$$

where

$$c_1=\frac{\begin{vmatrix}\delta_{01}&\delta_{12}\\ \delta_{02}&\delta_{22}\end{vmatrix}}{\begin{vmatrix}\delta_{11}&\delta_{12}\\ \delta_{12}&\delta_{22}\end{vmatrix}},\qquad c_2=\frac{\begin{vmatrix}\delta_{11}&\delta_{01}\\ \delta_{12}&\delta_{02}\end{vmatrix}}{\begin{vmatrix}\delta_{11}&\delta_{12}\\ \delta_{12}&\delta_{22}\end{vmatrix}} \tag{3.10}$$

with

$$\delta_{01}=\delta\gamma\,{}_0^i-\delta\gamma\,{}_1^i,\qquad \delta_{02}=\delta\gamma\,{}_0^i-\delta\gamma\,{}_2^i,$$

$$\delta_{11}=\delta\gamma\,{}_0^i-2\,\delta\gamma\,{}_1^i\delta\gamma\,{}_1^{i-1},\quad \delta_{22}=\delta\gamma\,{}_0^i-2\,\delta\gamma\,{}_2^i\delta\gamma\,{}_2^{i-1},$$

$$\delta_{12}=\delta\gamma\,{}_0^i-\delta\gamma\,{}_1^i\delta\gamma\,{}_2^i-\delta\gamma\,{}_2^{i-1}. \tag{3.11}$$

Actually the formula can be applied from the second iteration onwards defining $c_1=\delta_{01}/\delta_{11}$ and $c_2=0$ (i.e., applying a linear extrapolation). This implementation of Ng's algorithm has proven to be almost as rapidly convergent as Newton–Raphson algorithms, whereas it is extremely less complicated to program, since it simply involves storing three consecutive solutions and their correspondent deviations with respect to previous estimates, as indicated in Eq. (3.8). The increase in computer time per iteration with respect to simple direct substitution is negligible, whereas convergence is enhanced by factor of 50. On the other hand the implementation of this algorithm for mixtures, or two-band problems is trivial, quite opposite to what happens with Newton–Raphson or hybrid algorithms,[13] that even though still feasible in this mixture problem would be extremely complicated for multiple-band systems, especially when dealing with nonlinear closures.

Now we are left with the problem of the determination of Green's function from Eq. (2.8). This is also a non trivial problem that has to be solved in combination with Eqs. (2.9) and (2.10). In the case of one-component one-band fluids we have found that the most efficient procedure involves solving Eq. (2.8) for $G(z)$ in terms of z and the integral over the correlation functions (which is actually the self-energy of the system). This is easily done, with Eq. (2.8) in that case being a simple quadratic equation. In the present instance, however the situation is more involved, since Eq. (2.8) now forms a system of coupled quadratic equations which would have to be solved numerically for $\bar{G}^{\alpha\alpha}$ and $\bar{G}^{\beta\beta}$. This alternative is impractical, since this system in the vicinity of band edges is ill-conditioned due to the presence of multiple solutions that mark the onset of real solutions [i.e., $D(E)=0$]. It is possible however to write the equations in terms of self-energy defined by

$$S^{\alpha\alpha}=\sum_\lambda \rho_\lambda\bar{G}^{\lambda\lambda}\int V^{\alpha\lambda}(12)H^{\lambda\alpha}(21)d2 \tag{3.12}$$

and similarly for $S^{\beta\beta}$ (notice that there are no cross-Green's functions but cross correlations are present). Thus one gets $\bar{G}^{\alpha\alpha}=(z-S^{\alpha\alpha})^{-1}$ and $\bar{G}^{\beta\beta}=(z+\Delta\varepsilon-S^{\beta\beta})^{-1}$ where $\Delta\varepsilon=\varepsilon_\alpha-\varepsilon_\beta$ is the energy difference between levels α and β. We have found that the use of the self-energy form of the equation increases the stability of the solution procedure both in this problem and in the numerical of the solution at the two-band model.[14]

Now we can proceed as follows. Given initial estimates of $\bar{G}^{\alpha\alpha}$ and $\bar{G}^{\beta\beta}$, we solve the SSCA/EMA OZ Eqs. (2.9) and (2.10) to get $H^{\alpha\beta}$, the self energies are computed from Eq. (3.12) and determine a new set of $\bar{G}^{\alpha\alpha}$ and $\bar{G}^{\beta\beta}$. We are then back to the OZ step and one can proceed iteratively until convergence is achieved. The proposed scheme to solve for the Green's function is again suitable for the application of Ng's acceleration technique combined with a mixing iterates step. Notice that we can simply use Eqs. (3.8)–(3.11) in our new problem by just dropping the summation over r_j values. As a mater of fact this is nothing but a particular implementation of Brent's method for nonlinear algebraic equations.[15] Now since one has to solve for a more or less regular function of the energy, $D(E)$, a further improvement might be applied by using some sort of predictor–corrector method. If the Green's function values for a series of three consecutive energies are stored it is possible to use a parabolic extrapolation to predict the initial estimate corresponding to the following energy with great accuracy (the extrapolation can be performed both on $\bar{G}^{\alpha\alpha}$, $\bar{G}^{\beta\beta}$, and the correlations $H^{\alpha\beta}$). The method remarkably improves the performance, except in the vicinity of sharp band edges and peaks where the $D(E)$ is no longer smooth.

A final remark must be made concerning the numerical procedure. Both when dealing with the DOS of mixtures, and multiband systems, it is usual to find band gaps. In some cases the second band might actually start up abruptly in a band edge, i.e., the Green's functions, real in the band gap suddenly jump to complex values. This is typically associated with several real solutions meeting at the band edge precisely where the solution becomes complex. We have found this is an important source of numerical instability, which in some cases might prevent the convergence. On the order hand, the situation found here is completely analogous with the problem of the low density nonsolution region of the hypernetted chain (HNC) integral equation in simple fluids.[16] Following the ideas developed in Ref. 16 for the latter problem, it is possible to introduce an arbitrary imaginary perturbation in the equations for $\bar{G}^{\alpha\alpha}$ and $\bar{G}^{\beta\beta}$, such that the transition between real and imaginary solutions across the band edge is smoothed out (see Fig. 1 in Ref. 16). Thus solving for

$$\bar{G}^{\alpha\alpha}=(z-S^{\alpha\alpha}+i\chi)^{-1},\quad \bar{G}^{\beta\beta}=(z+\Delta\varepsilon-S^{\beta\beta}+i\chi)^{-1} \tag{3.13}$$

it is possible to get perturbed solutions corresponding to the second band, which might then be used as initial estimates

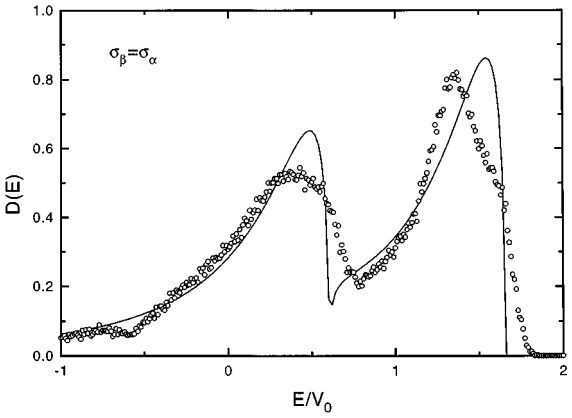

FIG. 2. Frequency spectra for an equimolar binary mixture at constant total density ($\rho\sigma_\alpha^3=0.2$) and $\sigma_\beta/\sigma_\alpha=1$. The Yukawa screening factor is $z=0.5\sigma_\alpha^3$. The simulation results are denoted by an open circle, and the solid line represents the SSCA/EMA theory.

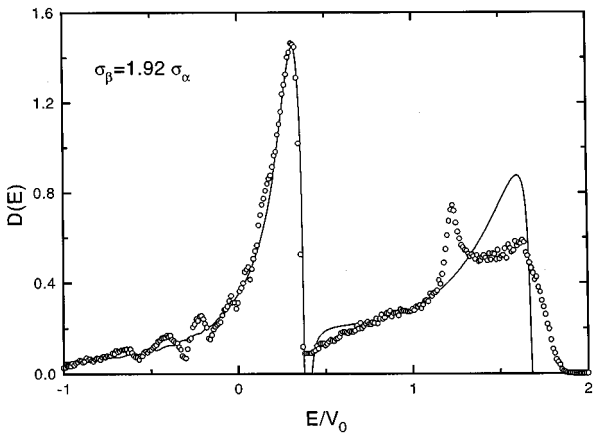

FIG. 4. Same as in Fig. 2 for $\sigma_\beta/\sigma_\alpha=1.92$.

for the unperturbed equation (i.e., for $\chi=0$). This trick works out nicely even in the most stubborn cases. We thus have all the ingredients required to solve the SSCA/EMA for our mixture problem. As for the details of the calculation, we have used 4096 grid points in r space with a grid size $\Delta r=0.05\sigma_\alpha$ in most cases. Some regions are particularly sensitive to range of integration in Eq. (3.12), and especially to the range in k space in the $\tilde{\Gamma}^{\alpha\beta}(k)$ entering Eq. (3.6), which is typically a very long-ranged function.

Now in Figs. 2–4 we present the DOS for our equimolar mixture of asymmetric hard spheres of total density $\rho\sigma_\alpha^3=0.2$ (σ_α taken as unit length) varying $\sigma_\beta/\sigma_\alpha$ from 1 to 1.92, which implies varying the total packing fraction $\eta=\pi/6(\rho_\alpha\sigma_\alpha^3+\rho_\beta\sigma_\beta^3)$ from 0.10 to 0.42. The values of the correlation functions inserted into the SSCA/EMA closure are taken from an integral equation for mixtures based on Verlet's approximation[17] which implements multiple thermodynamic consistency.[18] Distribution functions for the highest asymmetry are compared with Monte Carlo results in Fig. 5.

It must be mentioned that the changes introduced by the SSCA/EMA in the DOS with respect to the MSA solution are minimal, and would only be reflected by the second moments which are exactly reproduced when the spatial distribution function is properly included in the closure [let us recall that MSA is recovered from the SSCA/EMA by setting $g(r)$ in Eq. (2.10) equal to a step function]. One of the most representative results we can see in Figs. 2–4 is the increase in the height of the first peak with respect to the second as the ratio $\sigma_\beta/\sigma_\alpha$ is augmented. In other words, the contribution to the energy density of the β-type particles increases with their size. This is a purely geometric effect since the total number of electronically active sites (or oscillators if we use the picture of the fluid of coupled Drude oscillators) and the compositions are kept constant. The theoretical results predict the appearance of a gap as the size ratio increases which, according to the Monte Carlo results, can be expected to occur for somewhat higher asymmetries. This difference between the simulation and the theoretical results is easily

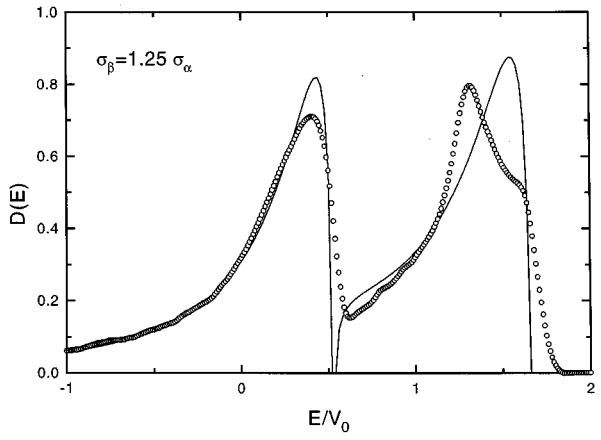

FIG. 3. Same as in Fig. 2 for $\sigma_\beta/\sigma_\alpha=1.25$.

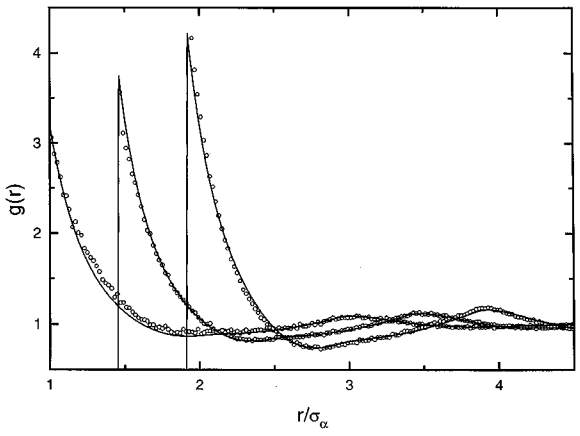

FIG. 5. Pair distribution functions for a hard-sphere mixture for the largest asymmetry considered in this work, $\sigma_\beta/\sigma_\alpha=1.92$. Open circles correspond to MC simulation and solid lines show the results from a self-consistent integral equation theory based on Verlet's approximation. (Refs. 17 and 18).

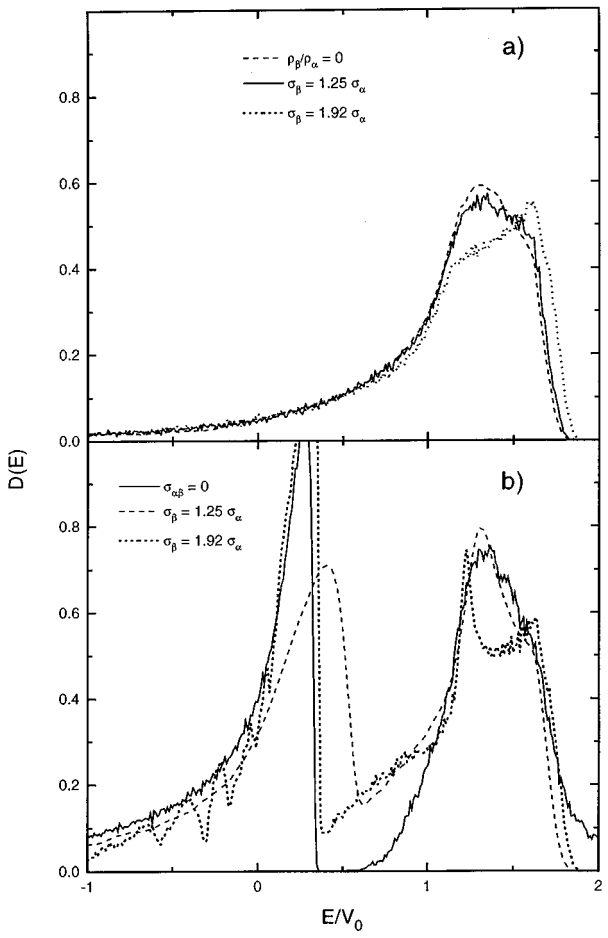

FIG. 6. (a) Simulated density of states for a mixture of electronically inactive hard spheres of diameter σ_β and hard spheres of diameter σ_α with a tight-binding Hamiltonian with Yukawa transfer matrix elements. The solid curve represents the results obtained in the absence of the β component. (b) Simulation results for the density of electronic states of a mixture of asymmetric hard spheres (size ratios 1:1.25 and 1:1.92 dashed and dotted lines, respectively) with a tight-binding Hamiltonian with Yukawa transfer matrix elements. The solid line represents the frequency spectra for the size ration 1:1.92 when particles of different types can penetrate each other.

understood as a consequence of the use of a linear approximation that misses the wings of the spectrum.[1,19] In this regard we expect that the use of a nonlinear closure like that of Eq. (2.12) might cure this deficiency.

Finally, the increase in the size ratio introduces an interesting new feature in the shape of the second band, i.e., the band corresponding to the component with the smallest size (α particles). When going from Fig. 2 to Fig. 4 we see that the second band undergoes a continuous transition and splits into two peaks as the size of the β particles is augmented. In order to understand the factors that come into play here, we have performed a set of simulations with the transfer matrix elements corresponding to β-type particles set to zero (i.e., the β-type Drude oscillators switched off). The DOS for this system with various size ratios can be seen in Fig. 6(a). Here we have also included results obtained in the absence of β particles. We see that for the largest size of the electronically inactive particles (which corresponds to a relatively highly packed state) there is a clear blueshift in the peak, but a shoulder is still present where the primitive peak was located. This change can easily be explained in terms of packing effects. As the size of β particles is increased and the system gets more packed, the smaller particles tend to form aggregates inside the cavities formed between the large spheres. The local density in these cavities is considerably larger than the average density and therefore this produces the shift to higher energy in the peak of the band. This blueshift in energy bands with increasing density is a well-known effect in disordered materials (see Fig. 7 in Ref. 9). The residual shoulder is very likely the result of intercavity electronic interactions. Now when considering what happens when the β particles are electronically active, we can see in Fig. 6(b) that the shape of the α band for the largest asymmetry [the dotted line in Fig. 6(b)] is very similar to that obtained for inactive β particles [the dotted line in Fig. 6(a)] except for the peak around $E/V_0 = 1.2$. Clearly this peak is due to the cross interaction between α and β electronic levels. This cross term also accounts for the the difference in height in the α band when the electronic levels of the β particles are turned off. We also performed an additional simulation for a system with the largest asymmetry, $\sigma_\beta/\sigma_\alpha = 1.92$, and the same transfer matrix elements considered in Figs. 2–4, but with the cross hard–core interaction $\sigma_{\alpha\beta}$ set to zero, i.e., now particles of different types can penetrate each other. This will of course remove all packing constrains on α particles, and hence we see in Fig. 6(b) (solid line) that despite the size asymmetry there is no longer any band splitting (nonetheless the height of the peak reflects the presence of the α–β transfer matrix elements in the Hamiltonian). A curious feature in these new simulation results is the fact that the system has now a band gap and the α band is more symmetric. So far, we lack an obvious explanation for this particular behavior.

As to the failure of the theory to reproduce these features, it can simply be attributed to the well-known inability of linear theories to properly account for effects whose origin is closely linked to the presence of strong inhomogeneities in the medium.

In summary, we have presented an extension of Logan and Winn's formalism to deal with the problem of mixtures of one-band fluids together with a set of efficient algorithms that enable the determination of its numerical solution. The results compared with Monte Carlo simulation for binary mixtures of asymmetric hard spheres with Yukawa type transfer matrix elements are qualitatively correct but also show the limitations inherent to linear approximations like the SSCA/EMA or MSA.

ACKNOWLEDGMENTS

The authors would like to thank Dr. M. D. Winn, for his very helpful suggestions and illuminating comments. This research was financially supported by the Spanish Dirección General de Investigación Científica y Técnica (DGICYT) under Grant No. PB94-0112.

[1] J. S. Høye, J. L. López Martín, and E. Lomba, J. Chem. Phys. **103**, 2178 (1995).
[2] J. S. Høye and E. Lomba, J. Chem. Phys. **101**, 4083 (1994).
[3] D. E. Logan and M. D. Winn, J. Phys. C **21**, 5773 (1988).
[4] M. D. Winn and D. E. Logan, J. Chem. Phys. **96**, 4818 (1992).
[5] M. D. Winn and D. E. Logan, J. Phys. Condens. Matter **1**, 8683 (1989).
[6] I. J. Bush, D. E. Logan, P. A. Madden, and M. D. Winn, J. Phys. Condens. Matter **1**, 8735 (1989).
[7] M. D. Winn (private communication).
[8] M. D. Winn and G. Kahl, J. Chem. Phys. **101**, 10850 (1994).
[9] C. F. Strnadl and G. Kahl, J. Phys. Condens. Matter **5**, 6801 (1993).
[10] K. Ganguly and R. M. Stratt, J. Chem. Phys. **95**, 4418 (1991); **97**, 1980 (1992).
[11] S. S. Jaswal and J. Hafner, Phys. Rev. B **38**, 7311 (1988).
[12] K. Ng, J. Chem. Phys. **61**, 2680 (1974).
[13] S. Labik, A. Malijevsky, and P. Vonka, Mol. Phys. **56**, 709 (1985).
[14] E. Lomba and J. L. López Martín (unpublished).
[15] W. H. Press, S. A. Teukolsky, W. T. Vetterling, and B. P. Flannery, *Numerical Recipes*, (Cambridge U. P. Cambridge, 1992) 2nd ed.
[16] E. Lomba and J. L. Lopez Martin, J. Stat. Phys. **80**, 825, (1995).
[17] L. Verlet, Mol Phys. **41**, 183 (1980).
[18] E. Lomba, M. Alvarez, L. L. Lee, and N. G. Almarza, J. Chem. Phys, **104**, 1 (1996).
[19] J. S. Høye, E. Lomba, and J. L. López Martín J. Chem. Phys. **101**, 9042 (1994).